Efficient antigen presentation by DCs requires regulated lysosomal protein degradation (*21*, *22*). However, the requirements for presentation on MHCII and cross-presentation on MHCI differ in that MHCII processing occurs inside endosomes, whereas cross-presentation on MHCI necessitates antigen escape from the endosome into the cytoplasm to gain access to the proteasome and TAP transporters (*19*, *20*, *23*–*25*). Elegant in vitro experiments with cultured DCs show that during DC development, antigen presentation is regulated through control of lysosomal processing and MHCII cell surface transport (*21*, *22*, *26*–*28*). Cultured immature DCs capture antigen but only process and present it on MHCII after exposure to inflammatory stimuli or TLR ligation (*22*). This unique ability to sequester antigens may be important for their preservation during DC transit from sites of inflammation to lymphoid organs and might facilitate the escape of antigen from endosomes to the cytoplasm or endoplasmic reticulum for cross-presentation (*21*). However, DCs that fail to degrade antigen might also be suboptimal producers of MHCII-p. Our experiments show that in the intact host, this problem is resolved by producing a subset of DCs specialized for maximizing MHCII presentation. Although $CD8^{+}DEC205^{+}$ DCs can initiate immune responses by presenting on MHCII, $CD8^{-}33D1^{+}$ DCs excel in producing MHCII-p. This specialization may have important implications for understanding the initiation of T cell responses in vivo and for rational vaccine design.

References and Notes

1. Y. J. Liu, *Cell* **106**, 259 (2001).
2. K. Shortman, Y. J. Liu, *Nat. Rev. Immunol.* **2**, 151 (2002).
3. R. M. Steinman, D. Hawiger, M. C. Nussenzweig, *Annu. Rev. Immunol.* **21**, 685 (2003).
4. D. Vremec *et al.*, *J. Exp. Med.* **176**, 47 (1992).
5. M. D. Witmer, R. M. Steinman, *Am. J. Anat.* **170**, 465 (1984).
6. R. S. Allan *et al.*, *Science* **301**, 1925 (2003).
7. J. M. den Haan, S. M. Lehar, M. J. Bevan, *J. Exp. Med.* **192**, 1685 (2000).
8. T. Iyoda *et al.*, *J. Exp. Med.* **195**, 1289 (2002).
9. J. M. den Haan, M. J. Bevan, *J. Exp. Med.* **196**, 817 (2002).
10. J. L. Pooley, W. R. Heath, K. Shortman, *J. Immunol.* **166**, 5327 (2001).
11. C. Scheinecker, R. McHugh, E. M. Shevach, R. N. Germain, *J. Exp. Med.* **196**, 1079 (2002).
12. P. Schnorrer *et al.*, *Proc. Natl. Acad. Sci. U.S.A.* **103**, 10729 (2006).
13. Materials and methods are available as supporting material on *Science* Online.
14. D. Hawiger *et al.*, *J. Exp. Med.* **194**, 769 (2001).
15. M. C. Nussenzweig, R. M. Steinman, M. D. Witmer, B. Gutchinov, *Proc. Natl. Acad. Sci. U.S.A.* **79**, 161 (1982).
16. L. Bonifaz *et al.*, *J. Exp. Med.* **196**, 1627 (2002).
17. G. Dadaglio, C. A. Nelson, M. B. Deck, S. J. Petzold, E. R. Unanue, *Immunity* **6**, 727 (1997).
18. M. Guo *et al.*, *Hum. Immunol.* **61**, 729 (2000).
19. P. Bryant, H. Ploegh, *Curr. Opin. Immunol.* **16**, 96 (2004).
20. P. Cresswell, N. Bangia, T. Dick, G. Diedrich, *Immunol. Rev.* **172**, 21 (1999).
21. L. Delamarre, M. Pack, H. Chang, I. Mellman, E. S. Trombetta, *Science* **307**, 1630 (2005).
22. E. S. Trombetta, I. Mellman, *Annu. Rev. Immunol.* **23**, 975 (2005).
23. R. N. Germain, *Cell* **76**, 287 (1994).
24. N. Shastri, S. Cardinaud, S. R. Schwab, T. Serwold, J. Kunisawa, *Immunol. Rev.* **207**, 31 (2005).
25. J. W. Yewdell, C. C. Norbury, J. R. Bennink, *Adv. Immunol.* **73**, 1 (1999).
26. K. Inaba *et al.*, *J. Exp. Med.* **191**, 927 (2000).
27. P. Pierre, I. Mellman, *Cell* **93**, 1135 (1998).
28. S. J. Turley *et al.*, *Science* **288**, 522 (2000).

29. We thank K. Velinzon for cell sorting; K.-H. Yao for technical assistance; H.-K. Lee, S. H. Park, and S. Y. Joe for help generating CD11c-hDEC205 mice; A. Flores-Langarica, S. Boscardin, A. Gazumyan, E. Besmer, and F. Nimmerjahn for helpful discussion; the MSKCC Monoclonal Antibody Core Facility for labeling of antibodies; and MSKCC Genomics Core Laboratory for performing the microarrays. Supported by grants from the NIH (to C.G.P., R.M.S., and M.C.N.). D.D. is a fellow of the Deutsche Forschungsgemeinschaft (DU 548/1-1), and V.R.B. was supported by the German National Academic Foundation. M.C.N. is an Investigator with the Howard Hughes Medical Institute. M.C.N. and R.M.S. are on the scientific advisory board of Celldex, a startup company interested in targeting dendritic cells.

Supporting Online Material

www.sciencemag.org/cgi/content/full/315/5808/107/DC1
Materials and Methods
Figs. S1 to S11
References

10 October 2006; accepted 15 November 2006
10.1126/science.1136080

Differential Transmission of Actin Motion Within Focal Adhesions

Ke Hu,* Lin Ji,* Kathryn T. Applegate, Gaudenz Danuser,† Clare M. Waterman-Storer†

Cell migration requires the transmission of motion generated in the actin cytoskeleton to the extracellular environment through a complex assembly of proteins in focal adhesions. We developed correlational fluorescent speckle microscopy to measure the coupling of focal-adhesion proteins to actin filaments. Different classes of focal-adhesion structural and regulatory molecules exhibited varying degrees of correlated motions with actin filaments, indicating hierarchical transmission of actin motion through focal adhesions. Interactions between vinculin, talin, and actin filaments appear to constitute a slippage interface between the cytoskeleton and integrins, generating a molecular clutch that is regulated during the morphodynamic transitions of cell migration.

Directed cell migration involves spatiotemporal orchestration of protrusion at the leading cell edge, adhesion of the protrusion to the extracellular matrix (ECM), pulling against the adhesions to translocate the cell body, and weakening of the adhesion at the cell rear for advancement (*1*). In this process, actin filaments (F-actin) must couple to the ECM through the plasma membrane (*1*–*3*) via focal adhesions (FAs) to translate actin polymerization and/or actin-myosin contraction into cell motion. FAs are complexes of >100 different proteins linking F-actin to clustered transmembrane integrin ECM receptors (*2*, *4*). Regulating the attachment between F-actin and integrins via proteins within FAs is thought to be critical for controlling the spatiotemporal variability of protrusion and traction (*5*) and the ability of cells to respond to mechanical cues.

It is well established that F-actin and FAs are coupled to each other. Many FA proteins bind directly or indirectly to F-actin (*6*–*8*) and/or integrins (*9*–*13*). Contractile actomyosin bundles are often rooted in FAs (*2*, *4*), and perturbations of actomyosin cause changes in FAs and vice versa (*2*). Although the importance of spatiotemporal coordination between FAs and F-actin in cell migration is well appreciated (*2*, *14*, *15*), it is not known which FA molecules interact with F-actin in living cells, and the dynamics of molecules within these two assemblies have never been analyzed simultaneously. Predicting how FA proteins behave in vivo by biochemical data alone is impossible because of the complexity of their interactions (*4*).

To study the dynamic interactions between F-actin and FAs, we combined total internal reflection fluorescence microscopy (TIRFM) and fluorescent speckle microscopy (FSM). TIRFM optimizes image contrast at the ventral cell–ECM/coverslip interface where cortical F-actin integrates with FAs. FSM marks macromolecular assemblies with fluorophore clusters called speckles (fig. S1). Computational tracking of speckle motion allows mapping of protein dynamics with submicron resolution (*16*, *17*). We studied PtK1 cells migrating on coverslips, on which they organized a fibronectin-containing ECM (fig. S2).

To determine the spatial relations between FAs and F-actin flow, we captured image pairs using TIRFM of green fluorescent protein

Department of Cell Biology, The Scripps Research Institute, La Jolla, CA 92037, USA.

*These authors contributed equally to this work.
†To whom correspondence should be addressed. E-mail: waterman@scripps.edu (C.M.W.-S.); gdanuser@scripps.edu (G.D.)

(GFP)–vinculin and TIR-FSM of X-rhodamine actin (Fig. 1). As seen previously (*16*), the narrow meshwork of F-actin in the lamellipodium underwent rapid retrograde flow from the leading edge toward the cell center. Proximal to this, F-actin retrograde flow in the lamella was slower. An overlay of FAs onto the F-actin flow map revealed that the negative flow speed gradient at the lamellipodium/lamella junction corresponded to the distal boundaries of FAs (Fig. 1, C and D). Thus, FAs may locally dampen flow by engaging F-actin to the ECM. The global slowing of F-actin flow in the lamella is probably due to the uniform distribution of FAs and the small inter-FA spacing in this cell region. Despite the slowing, F-actin retrograde flow within FAs was substantial and coherent (Fig. 1C) (*18*). Thus, if an interaction between FA proteins and F-actin occurs in living cells, movement of proteins within FAs is likely.

To analyze the motion of proteins within FAs, we performed TIR-FSM on cells expressing three classes of GFP-conjugated FA proteins: first, a fibronectin-binding integrin (GFP–α_v integrin coexpressed with untagged β_3 integrin); second, FA proteins capable of binding directly to F-actin [α-actinin (*6*), vinculin (*8*, *19*), and talin (*6*, *20*)]; and third, FA "core" proteins that do not bind F-actin or the ECM directly but include structural and signaling molecules [paxillin (*9*, *21*), zyxin (*12*), and focal-adhesion kinase (FAK) (*13*)]. We focused on FAs in the ~100-nm-thick leading-edge lamella, where F-actin forms transverse bundles, isotropic networks, and stress fibers (*22*), all of which are within the evanescent excitation field. FA speckles were tracked within segmented FA regions, and average speckle speeds and coherencies were computed (*18*). Monte Carlo simulations showed that random binding and dissociation of fluorescent molecules to and from an immobile FA produced speckle velocities <0.05 μm/min and coherencies <0.4 on a scale of 0 to 1 (fig. S7), similar to measurements of X-rhodamine–actin speckles imaged in a fixed cell (*18*) and thus defining the detection limit of our measurements.

We found highly diverse behaviors of the seven GFP–FA proteins within FAs (Fig. 2 and tables S1 and S2). Speckles consisting of FA proteins with no known F-actin–binding activity moved slowly and mostly incoherently (Fig. 2, movies S1 to S3, and tables S1 and S2). Of these, GFP–$\alpha_v\beta_3$ integrin was the slowest and the most incoherent (Fig. 2C and movie S1), probably due to its immobilization by binding to the ECM on the coverslip. FA core proteins were slightly more motile than $\alpha_v\beta_3$ integrin, with a retrograde directional bias in their movement (Fig. 2, D to F). GFP-zyxin and GFP-paxillin moved somewhat more coherently than GFP–$\alpha_v\beta_3$ integrin, whereas GFP-FAK speckles moved faster than GFP–$\alpha_v\beta_3$ integrin (Fig. 2, D to F; movie S2; and tables S1 and S2).

In contrast, all three GFP-tagged FA actin–binding proteins moved coherently within the FAs. The dynamics of FA actin–binding proteins were significantly different from those of both the

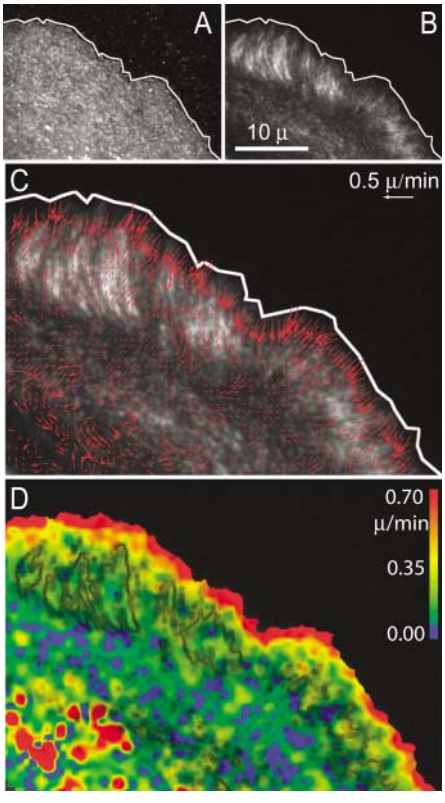

Fig. 1. F-actin motion relative to FAs at the leading edge of a migrating PtK1 epithelial cell. (**A**) TIR-FSM image of X-rhodamine actin and (**B**) TIRF image of GFP-vinculin. (**C**) Velocity vectors of F-actin speckle motion averaged over 100 s are overlaid on the TIRF image of GFP-vinculin. (**D**) Color-coded map of F-actin speed, with FAs outlined in gray.

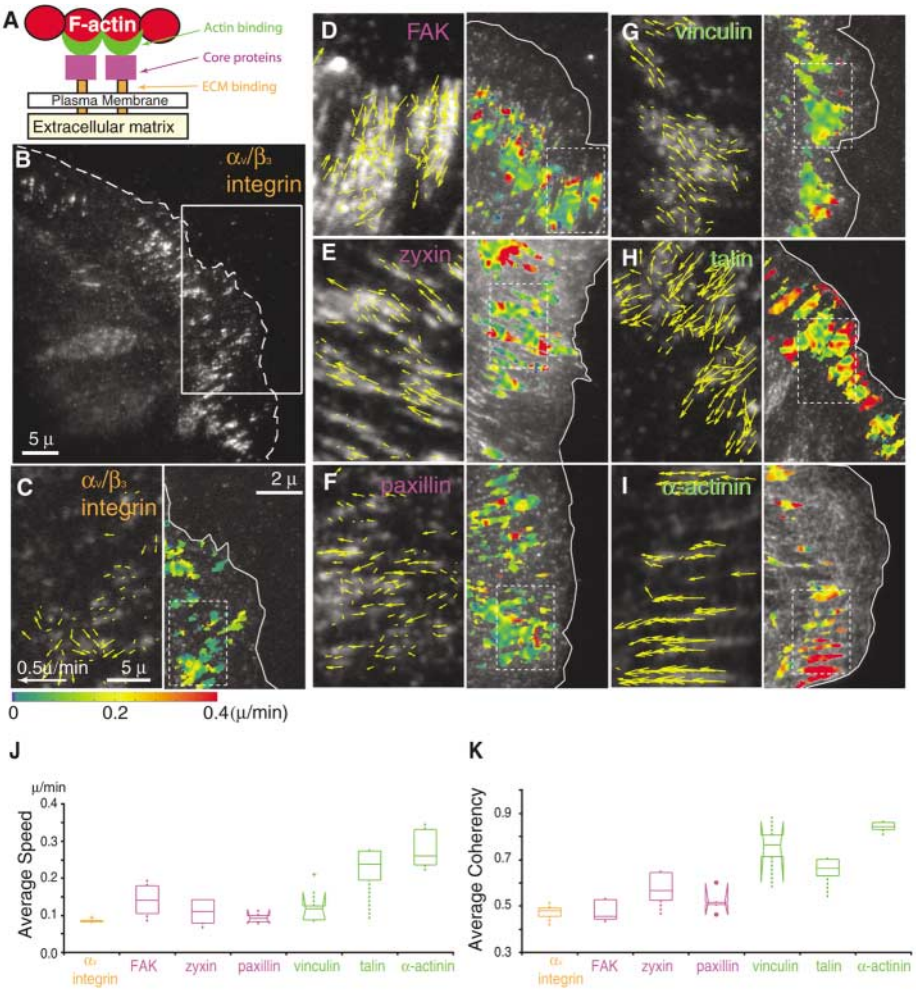

Fig. 2. The motions of different proteins within FAs are diverse. (**A**) Classes of FA molecules analyzed. FA-actin–binding proteins, green; FA core proteins, purple; integrins, orange. (**B**) TIR-FSM image of a cell coexpressing GFP–α_v integrin and untagged β_3 integrin. White frame, region shown in (C), on the right. (**C** to **I**) Velocity vectors (left) and speed maps (right, boxed area shown at left) of seven GFP-tagged FA proteins analyzed by TIR-FSM. (**J** and **K**) Average speed and velocity coherency of FA molecules [also see tables S1 and S2 (*18*) and fig. S3A].

integrin and core proteins and also from each other (Fig. 2, G to I; movie S3; and tables S1 and S2). GFP–α-actinin speckles moved fastest and most coherently. GFP-vinculin speckles moved slowly but highly coherently, whereas GFP-talin speckle motion was the least coherent of all three, but it was significantly faster than vinculin. Speed maps revealed that speckle speeds could vary within individual FAs and between adjacent FAs (Fig. 2, C to I). None of these FA proteins possess motor activity or interact with motor proteins, which suggests that their motion is influenced by interactions with other dynamic cell components, such as F-actin.

To determine whether the motion of proteins within FAs was related to F-actin flow, we developed correlational FSM to quantify the degree of motion correlation between GFP-FA and X-rhodamine–F-actin speckles (*18*). As verified by Monte Carlo simulations, a high degree of speckle motion correlation indicates concerted movement of molecules as part of the same macromolecular ensemble, mediated by direct or indirect interactions. We tracked speckle motion within FAs in both channels and interpolated speckle velocities onto a common 0.45-μm–by–0.45-μm grid to allow comparison of pairs of FA and F-actin flow vectors (fig. S3).

To determine the dependency between the velocities of FA protein and F-actin speckles, we performed linear regression of scatter plots of FA versus F-actin speckle velocities averaged within individual FAs (Fig. 3A and fig. S5A). This revealed velocity correlations between F-actin and the FA actin–binding proteins vinculin, α-actinin, and talin. The relatively low correlation coefficient for talin indicated a high variability in the talin–F-actin interaction.

To estimate the extent of molecular coupling between F-actin and FA molecules, we computed two parameters: direction coupling score (DCS = cos θ, where θ is the angle between paired FA and F-actin vectors), to measure the directional similarities between FA and F-actin speckle motions, and velocity magnitude coupling score (VMCS) (Fig. 3B and fig. S3), to measure relative FA speckle motion along the local F-actin flow axis, thus accounting for both direction and speed. For identical speckle flow fields, both DCS and VMCS are equal to 1 (see Fig. 3, G to H; tables S3 to S5; and fig. S4 for analysis of GFP- and Alexa 568–actin in the same cell).

Analysis of FAs in the lamella revealed that couplings between different FA molecules and F-actin were highly diverse (tables S4 and S5). FA core proteins and $\alpha_v\beta_3$ integrin both exhibited a DCS and a VMCS much less than 1 (Fig. 3, fig. S5, movies S5 to S8, and tables S4 and S5). Therefore, a substantial portion of the motion of

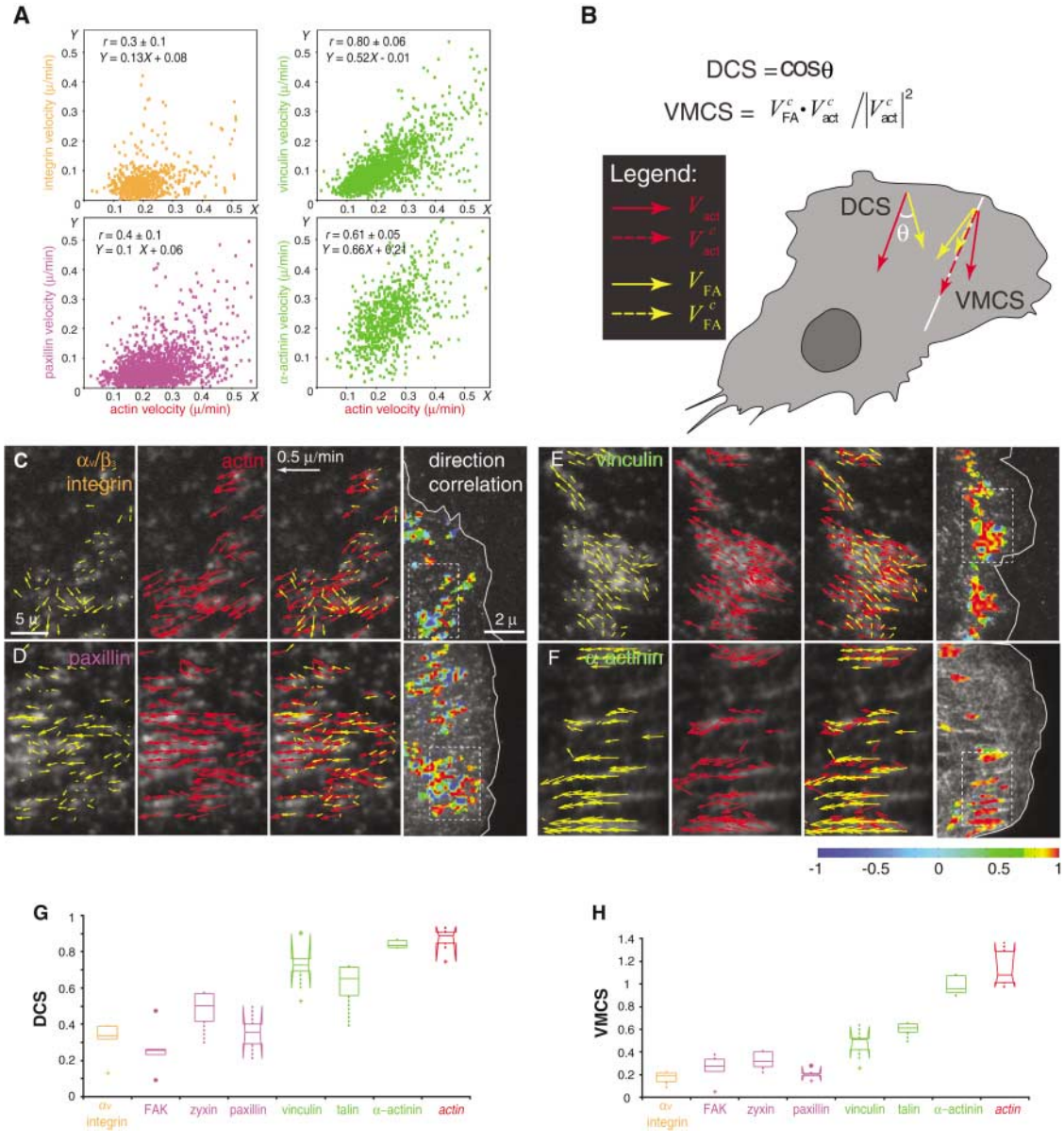

Fig. 3. Correlational FSM reveals that proteins within FAs are differentially coupled to F-actin motion. (**A**) FA versus F-actin speckle motions. Each point represents the average FA and F-actin speckle velocities within one FA at one time step. Correlation coefficients (*r*) and two times the standard deviation are indicated (bootstrap regression, 200 trials). *Y*, FA protein velocity; *X*, F-actin velocity. (**B**) Definitions of DCS and VMCS [also see (*18*) and fig. S3]. V_{FA} and V_{act} are the actual velocity measurements, and V^c_{FA} and V^c_{act} are the coupled components of the flow vectors. (**C** to **F**) Correlational FSM analysis of GFP–$\alpha_v\beta_3$ integrin (C), paxillin-GFP (D), vinculin-GFP (E), and α-actinin–GFP (F). From left to right in each panel are FA speckle velocity, F-actin speckle velocity, an overlay of the two velocities, and a color-coded DCS map. (**G** and **H**) Average DCS (G) and VMCS (H) between FA molecules and F-actin (averages from several cells, tables S4 and S5). Red, scores for a cell containing GFP-actin and Alexa 568–actin (fig. S4).

FA core proteins and $\alpha_v\beta_3$ integrin was not related to F-actin flow but was probably caused by interactions with other binding partners within FAs that immobilize them or deviate their motion from the F-actin flow axis. Alternatively, binding and dissociation of FA proteins to and from FAs could also generate random minor speckle displacements (figs. S6 and S7).

The motions of FA actin–binding proteins within FAs all showed significantly greater coupling to F-actin motion than did core proteins and $\alpha_v\beta_3$ integrin, although they were clearly different from each other (movies S9 to S11 and tables S4 and S5). α-Actinin displayed the highest coupling to F-actin motion (movie S11). This is expected because α-actinin mimics the kinematics of F-actin throughout the cell, indicating its tight association with F-actin, irrespective of localization (*23*, *24*). Both vinculin and talin were significantly, yet partially, coupled to F-actin motion, indicating partial transmission of F-actin motion to these proteins within FAs (tables S4 and S5).

Mapping local DCS revealed heterogeneity in coupling between F-actin and FA proteins within individual FAs and between adjacent FAs (Fig. 3, C to F). To see whether this heterogeneity was related to whole-FA dynamics or cell migration behavior, we performed correlational FSM for vinculin and F-actin (Fig. 4A and movie S12) at the leading edge of a cell where one area protruded and an adjacent area retracted (Fig. 4A). The protrusive area contained a FA that remained stationary, whereas the FA in the retracting area slid rearward and later stabilized (Fig. 4A). In the stationary FA, the speeds of F-actin and vinculin speckle flow and the DCS and VMCS between F-actin and vinculin remained relatively constant, with only small fluctuations over time (Fig. 4B). In contrast, in the sliding FA, the speeds of actin and vinculin and their VMCS and DCS increased before FA sliding (Fig. 4C). The coupling between vinculin and F-actin peaked during FA sliding and decreased before FA stabilization. Thus, dissociation of vinculin from a less mobile FA component and stable vinculin–F-actin binding may initiate FA disengagement from the ECM, whereas partial coupling between vinculin and F-actin may be necessary for establishing and/or maintaining the engagement between the FA and the ECM.

Our direct analysis of the dynamic interactions between FA components and F-actin in living cells reveals that the efficiency of motion transmission from F-actin to FA proteins within FAs decreased from actin-binding proteins to FA core proteins to integrin, defining a hierarchical slippage clutch. This is likely to be the result of differential transmission of F-actin–based force through a network of transient protein-protein interactions in FAs. Partial coupling of talin and vinculin to F-actin motion could represent these molecules spending part of

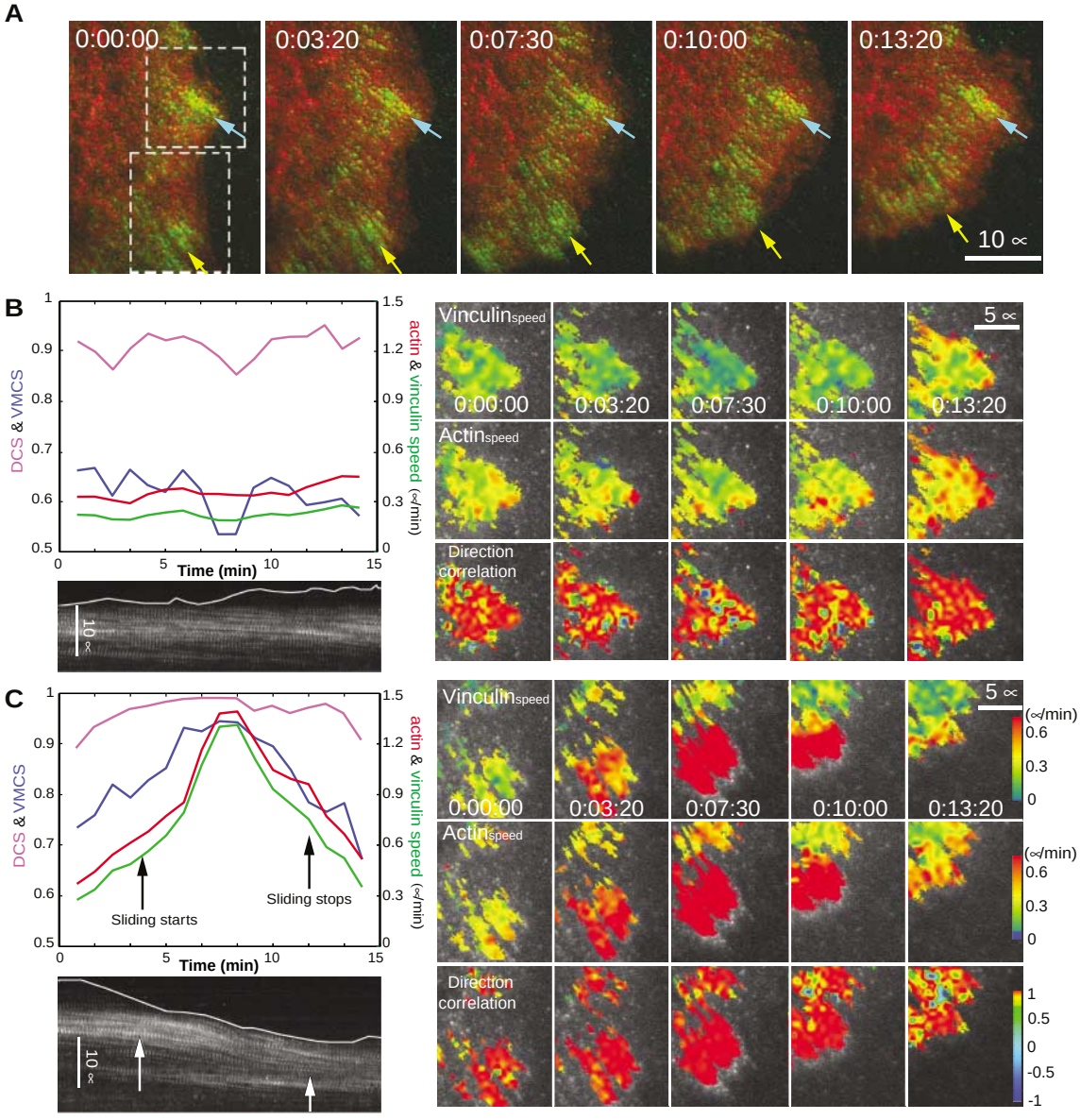

Fig. 4. Vinculin–F-actin coupling is time-modulated during the retraction of a FA. (**A**) Images of GFP-vinculin (green) and X-rhodamine–actin (red). Blue arrow, stable FA in a protrusive cell region; yellow arrow, sliding FA in a retracting cell region; white frames, regions of interest analyzed by FSM in (B) and (C). (**B** and **C**) Temporal variation of F-actin and vinculin speckle speeds, DCS, and VMCS within a stable (B) and a sliding (C) FA. Top left panels show graphs of average speeds of F-actin (red) and vinculin (green) speckles, vinculin-actin VMCS (blue), and vinculin-actin DCS (pink). Bottom left panels show kymographs of GFP-vinculin taken along the axes of arrows in (A). The position of the cell edge in white shows that the FA remains stationary in (B), whereas in (C) the FA initiates sliding at ~4 min (left arrow) and stops at ~12 min (right arrow). Right panels show maps of vinculin and actin speckle speeds and DCS. During retraction and FA sliding, vinculin alters its binding to F-actin. Time is given in hour:min:sec.

their time bound to moving F-actin and part of their time bound to a less mobile FA component, thus identifying these proteins as a site of slippage in the F-actin/FA interface. Alternatively, differential coupling of FA proteins to transverse actin bundles and stress fibers in the lamella could contribute to the observed effect. However, given the local slowing of F-actin flow in the FA in the lamella and the biophysical evidence implicating talin and vinculin in force transmission in the FA (*20*, *25*, *26*), we suspect that these proteins form transient linkages across the slippage interface, resulting in force-transducing slip-stick friction between F-actin and the ECM. The degree of molecular motion transmission through the FA was regulated, and it was correlated with protrusion and retraction events during cell migration. Therefore, FA internal molecular kinematics may be a key element in the integrin-mediated translation of intracellular biochemistry into cellular mechanics during cell and tissue morphogenesis, or in the reception of extracellular mechanical signals to mediate sensory perception, tissue maintenance, and differentiation (*27*).

References and Notes

1. D. A. Lauffenburger, A. F. Horwitz, *Cell* **84**, 359 (1996).
2. K. Burridge, M. Chrzanowska-Wodnicka, *Annu. Rev. Cell Dev. Biol.* **12**, 463 (1996).
3. C. H. Lin, P. Forscher, *Neuron* **14**, 763 (1995).
4. B. Geiger, A. Bershadsky, R. Pankov, K. M. Yamada, *Nat. Rev. Mol. Cell Biol.* **2**, 793 (2001).
5. R. J. Pelham Jr., Y. Wang, *Proc. Natl. Acad. Sci. U.S.A.* **94**, 13661 (1997).
6. K. Maruyama, S. Ebashi, *J. Biochem. (Tokyo)* **58**, 13 (1965).
7. M. Muguruma, S. Matsumura, T. Fukazawa, *Biochem. Biophys. Res. Commun.* **171**, 1217 (1990).
8. R. P. Johnson, S. W. Craig, *Nature* **373**, 261 (1995).
9. T. Tanaka, R. Yamaguchi, H. Sabe, K. Sekiguchi, J. M. Healy, *FEBS Lett.* **399**, 53 (1996).
10. D. A. Calderwood *et al.*, *J. Biol. Chem.* **274**, 28071 (1999).
11. K. Burridge, P. Mangeat, *Nature* **308**, 744 (1984).
12. M. C. Beckerle, *Bioessays* **19**, 949 (1997).
13. D. D. Schlaepfer, T. Hunter, *Cell Struct. Funct.* **21**, 445 (1996).
14. K. M. Yamada, S. Miyamoto, *Curr. Opin. Cell Biol.* **7**, 681 (1995).
15. M. Chrzanowska-Wodnicka, K. Burridge, *J. Cell Biol.* **133**, 1403 (1996).
16. A. Ponti, M. Machacek, S. L. Gupton, C. M. Waterman-Storer, G. Danuser, *Science* **305**, 1782 (2004).
17. L. Ji, G. Danuser, *J. Microsc.* **220**, 150 (2005).
18. Materials and methods are available as supporting material on *Science* Online.
19. B. Geiger, *Cell* **18**, 193 (1979).
20. G. Jiang, G. Giannone, D. R. Critchley, E. Fukumoto, M. P. Sheetz, *Nature* **424**, 334 (2003).
21. C. E. Turner, J. R. Glenney Jr., K. Burridge, *J. Cell Biol.* **111**, 1059 (1990).
22. S. L. Gupton *et al.*, *J. Cell Biol.* **168**, 619 (2005).
23. M. Edlund, M. A. Lotano, C. A. Otey, *Cell Motil. Cytoskelet.* **48**, 190 (2001).
24. G. Giannone *et al.*, *Cell* **116**, 431 (2004).
25. R. M. Ezzell, W. H. Goldmann, N. Wang, N. Parasharama, D. E. Ingber, *Exp. Cell Res.* **231**, 14 (1997).
26. G. Giannone, G. Jiang, D. H. Sutton, D. R. Critchley, M. P. Sheetz, *J. Cell Biol.* **163**, 409 (2003).
27. A. Katsumi, A. W. Orr, E. Tzima, M. A. Schwartz, *J. Biol. Chem.* **279**, 12001 (2004).

28. We thank C. Otey (University of North Carolina, Chapel Hill), A. Huttenlocher (University of Wisconsin, Madison), D. Schlaepfer (Scripps), A. F. Horwitz (University of Virginia, Charlottesville), I. Kaverina (Vanderbilt University), and M. Ginsberg (University of California, San Diego) for complementary DNAs. Supported by NIH grants GM67230 (C.M.W.-S. and G.D.) and U54GM64346 (G.D. and L.J.), American Heart Association Established Investigatorship and NIH Director's Pioneer Award (C.M.W.-S.), Leukemia and Lymphoma Society (K.H.), and NSF (K.T.A.).

Supporting Online Material

www.sciencemag.org/cgi/content/full/315/5808/111/DC1
Materials and Methods
Figs. S1 to S8
Tables S1 to S5
References
Movies S1 to S14

13 September 2006; accepted 16 November 2006
10.1126/science.1135085

Live-Cell Imaging of Enzyme-Substrate Interaction Reveals Spatial Regulation of PTP1B

Ivan A. Yudushkin,[1]* Andreas Schleifenbaum,[1]* Ali Kinkhabwala,[1]* Benjamin G. Neel,[2] Carsten Schultz,[1] Philippe I. H. Bastiaens[1]†

Endoplasmic reticulum–localized protein-tyrosine phosphatase PTP1B terminates growth factor signal transduction by dephosphorylation of receptor tyrosine kinases (RTKs). But how PTP1B allows for RTK signaling in the cytoplasm is unclear. In order to test whether PTP1B activity is spatially regulated, we developed a method based on Förster resonant energy transfer for imaging enzyme-substrate (ES) intermediates in live cells. We observed the establishment of a steady-state ES gradient across the cell. This gradient exhibited robustness to cell-to-cell variability, growth factor activation, and RTK localization, which demonstrated spatial regulation of PTP1B activity. Such regulation may be important for generating distinct cellular environments that permit RTK signal transduction and that mediate its eventual termination.

Protein-tyrosine phosphorylation is widely used by eukaryotic cells to transduce signals, but the dynamic interplay between receptor tyrosine kinases (RTKs) and protein-tyrosine phosphatases (PTPs) remains poorly understood (*1*, *2*). The protein tyrosine phosphatase–1B (PTP1B) resides on the surface of the endoplasmic reticulum (ER) (*3*, *4*) and helps terminate signaling by multiple RTKs, including the epidermal growth factor receptor (EGFR) (*5*). Previous reports demonstrate that RTK signaling occurs at the plasma membrane and endosomes (*6*), and its termination occurs along the ER surface (*7*–*11*). Because PTP1B has much higher specific activity than typical RTKs in vitro (*12*, *13*), uniformly high PTP1B activity along the ER could prevent endosomal RTK signaling. To account for compartmentalized RTK signaling, we hypothesized that PTP1B might exist inside cells as spatially separated subpopulations with different kinetic properties.

To test this hypothesis, we developed an imaging approach based on Förster resonant energy transfer (FRET) to spatially resolve enzyme-substrate (ES) interactions and thereby to monitor enzyme activity in live cells (Fig. 1A) (*11*). We tagged PTP1B with a donor chromophore by fusion to a genetically encoded fluorescent protein, and conjugated the substrate, a synthetic phosphotyrosine-containing peptide, to an acceptor chromophore (Fig. 1B). For Michaelis-Menten kinetics, the steady-state fraction (α) of ES complex to total enzyme (E_0) is as follows:

$$\alpha = ES/E_0 = S/(K_M + S) \qquad (1)$$

where S is the substrate concentration, and K_M is the Michaelis-Menten constant. The fraction α can be mapped across the cell by quantitatively imaging FRET with the use of fluorescence lifetime imaging microscopy (FLIM) (*14*–*16*).

We first tested whether formation of the ES intermediate could be detected by FRET in vitro. To stabilize the ordinarily transient ES intermediate and thereby to facilitate FRET detection, we used the purified enhanced green fluorescent protein (EGFP)–tagged catalytically impaired mutant of PTP1B that retains substrate-binding ability (residues 1 to 321, $PTP1B^{D181A}$, in which Ala^{181} was substituted for Asp) (*17*, *18*). Indeed, FRET in the ES complex was apparent, as in-

[1]European Molecular Biology Laboratory (EMBL), Meyerhofstrasse 1, D-69117 Heidelberg, Germany. [2]Cancer Biology Program, Division of Hematology-Oncology, Department of Medicine, Beth Israel Deaconess Medical Center, Harvard Medical School, 77 Avenue Louis Pasteur, Boston, MA 02115, USA.

*These authors contributed equally to this work.
†To whom correspondence should be addressed. E-mail: bastiaen@embl.de